Am J Nucl Med Mol Imaging 2019;9(3):185-192
www.ajnmmi.us /ISSN:2160-8407/ajnmmi0094541

Original Article

The relationship between tumor aggressiveness and cholinergic PET imaging in prostate cancer tissue. A proof-of-concept study

Maria M Nielsen[1], Lars P Tolbod[1], Michael Borre[2], Søren Høyer[3], Hendrik J Harms[1], Jens Sørensen[1], Jørgen Frøkiær[1], Per Borghammer[1]

Departments of [1]Nuclear Medicine and PET, [2]Urology, [3]Pathology, Aarhus University Hospital, Aarhus, Denmark

Received March 28, 2019; Accepted April 22, 2019; Epub June 15, 2019; Published June 30, 2019

Abstract: It was recently shown that high-risk prostate carcinoma (PCa) exhibited parasympathetic neurogenesis. The PET tracer ^{11}C-donepezil is a marker of parasympathetic innervation. Therefore, we studied if parasympathetic nerve density in PCa measured with ^{11}C-donepezil PET correlated with PCa aggressiveness and if metastases could be visualized. Twenty-six patients were included into three groups with varying tumor aggressiveness. Dynamic and static PET scans were performed. Maximal standardized uptake values (SUV_{max}) were determined in lesions within the prostate, lymph nodes, and bones. SUV_{max} in primary PCa were compared between groups, and comparisons between SUV_{max} and Gleason score and Prostate-specific antigen (PSA) were performed. Kinetic modelling was performed and time-activity curves of healthy tissue and tumor tissue fitted and compared. Tumor kinetic parameters were normalized to those of healthy tissue producing ratios of K1 and k2. Median SUV_{max} in primary PCa was higher in high-grade compared to low-grade PCa (P = 0.052). No correlation was seen between Gleason score and SUV_{max} (P = 0.28). A trend-level correlation was seen between PSA and SUV_{max} (P = 0.078). Median SUV_{max} was 7.7 (4.7-22.5) for suspected lymph node metastases and 8.2 (5.4-14.8) for suspected bone metastases. A significant difference was seen between time-activity tissue curves for low- and high-grade PCa (P = 0.012). Highly significant differences were seen in K1- and k2-ratios between low- and high-grade PCa (P = 0.0006 and P < 0.0001). We showed that ^{11}C-donepezil accumulates in primary PCa and metastases. Simple SUV_{max} values of the cancer hot spots were higher in high-risk tumors compared to low-risk tumors. Further studies should elucidate the importance of cholinergic neurogenesis for prostate cancer biology.

Keywords: PET, prostate cancer, parasympathetic, cholinergic

Introduction

Prostate carcinoma (PCa) accounts for 19% of all cancer cases among men and is the third deadliest cancer amounting for 8% of all cancer deaths [1]. PCa is demonstrated in 63% of autopsies in men aged 60-69 years and the prevalence increases markedly with age [2]. Radical prostatectomy confers a lower PCa mortality, but only in patients with prostate-specific antigen (PSA) values > 10 ng per mL or high-risk PCa [3].

The PCa diagnosis and pre-treatment stratification into low, intermediate, and high-risk groups are based on three methods: Digital rectal examination, PSA, and transrectal ultrasound guided needle biopsies (TRUSb), with the latter being the gold standard for providing histological diagnosis [4]. However, random biopsies have several disadvantages including the underestimation of Gleason scores in ~40% of cases and false negative biopsies in up to 20% of cases depending on the biopsy protocol [5, 6].

Consequently, there is a need for improved diagnostic tools to select patients with aggressive disease for local therapy and patients with less aggressive disease for active surveillance. Novel molecular imaging markers and imaging techniques provide an attractive strategy to examine patients with PCa non-invasively.

The normal prostate is innervated with autonomic nerve fibres in the capsule and the parenchyma [7, 8]. A recent study demonstrated that neurogenesis of autonomic nerves may be of key importance in PCa biology. The authors showed that high-risk PCa displayed a 110% increase in parasympathetic nerve fibre density in tumor tissue compared to low-risk PCa. Increased density of parasympathetic nerves in tumors was predictive of poor survival. Moreover, in PCa animal models pharmacological blockade of parasympathetic muscarinic receptors significantly inhibited metastases formation and lead to improved survival [9]. Thus, parasympathetic neurogenesis seems to be involved in tumor aggressiveness and the propensity to form metastases.

We recently validated the acetylcholinesterase (AChE) ligand, [5-^{11}C-methoxy]donepezil, for in vivo quantification of cholinergic nerve density. AChE is mainly found in cholinergic nerve terminals, where it hydrolyses the neurotransmitter acetylcholine, and ^{11}C-donepezil may therefore serve as a measure of parasympathetic innervation [10, 11]. Furthermore, using ^{11}C-donepezil autoradiography, we investigated 13 prostatectomy specimens and demonstrated significantly higher ^{11}C-donepezil uptake in high-risk PCa compared to low-risk PCa [12].

In the present proof-of-concept study, we studied 26 PCa patients with ^{11}C-donepezil PET/CT and hypothesized that the ^{11}C-donepezil uptake in primary PCa would correlate with the degree of malignancy. In addition, we included a patient subgroup with known or high probability of metastases to examine the ^{11}C-donepezil uptake in metastases.

Methods

Participants

26 patients with confirmed or suspected PCa were recruited from the Department of Urology at Aarhus University Hospital and stratified into three groups. Group I (n = 10) consisted of patients with high probability of low grade cancer, i.e. PCa localized to the prostate. These patients did not undergo any active treatment. Protocol inclusion criteria were PSA < 20 mg/ml, clinical stage < T3, and biopsy based Gleason score ≤ 7. However, three patients had a biopsy based Gleason score of 8, but all had bone scintigraphy or choline PET/CT to exclude lymph node and bone metastases. The PET scan was performed > 8 weeks after biopsy, as TRUSb may be associated with a local inflammatory tissue reaction potentially giving rise to inflammation related ^{11}C-donepezil uptake.

Group II (n = 8) comprised patients under suspicion of high grade PCa at the time of diagnosis. The patients were referred to the department with PSA > 50 ng/ml. Patients were recruited and PET scanned prior to TRUSb or any surgical or medical treatment. Subsequently, Gleason scores and other relevant clinical data were extracted from patient records.

Group III (n = 8) patients had verified castration-resistant PCa and increasing PSA values or known metastatic disease. They all received androgen deprivation therapy (ADT), and were PET scanned in the study before any oncological treatment. The primary aim of including group III was to study whether ^{11}C-donepezil showed appreciable binding to lymph node metastases and bone metastases.

Exclusion criteria for all groups were major organ failure, decreased kidney function, liver cirrhosis, previous or current cancers others than PCa, use of cholinergic medications and previous allergic reactions to CT contrast. The study was approved by the Science Ethics Committee of the Central Region of Denmark prior to its inception.

^{11}C-donepezil PET/CT scan

All patients fasted for a minimum of 6 hours prior to PET. A catheter was inserted in the anterior cubital vein for injection of ^{11}C-donepezil and intra-venous (i.v.) CT contrast. The chemical structure of [5-^{11}C-methoxy] donepezil is shown in **Figure 1A**. The radiochemical synthesis has been previously described in detail [10]. Median specific activity of ^{11}C-donepezil was 120 GBq/μmol (inter-quartile range 79-200) and the radiochemical purity was 99.9% (inter-quartile range 99.8-99.9%). Before initiation of PET a low-dose CT scan of the pelvis was performed for attenuation correction and anatomical localization. ^{11}C-donepezil was manually injected, and the median dose was 508 MBq (range 319-634). During the first dynamic PET scan (36 min) the prostate was in field-of-view (FOV). 32 frames were obtained with increasing

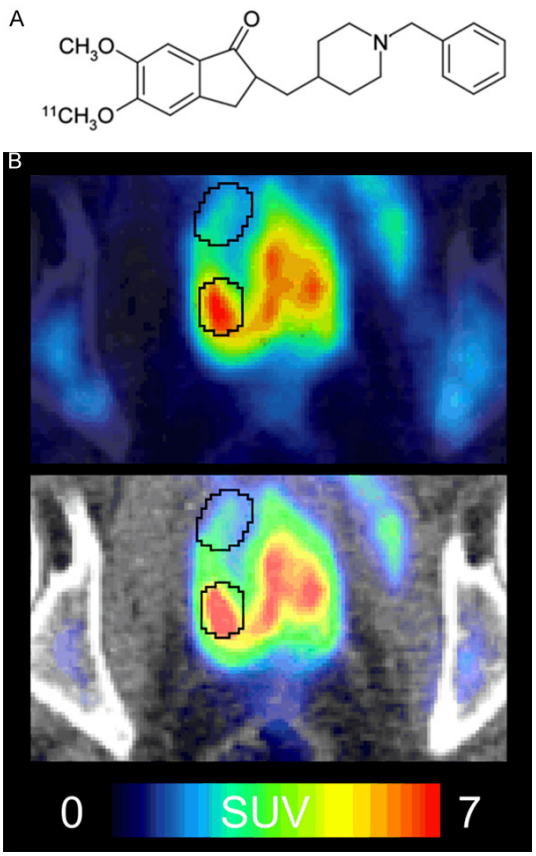

Figure 1. A. Chemical structure of [5-^{11}C-methoxy] donepezil. B. Volumes of interest (VOIs) from a representative patient with high-risk PCa. VOIs were placed on the most tracer-avid hot spot and on reference prostate tissue with low magnitude tracer avidity. [Summed PET image from 24-32 min post-injection].

frame durations (12 × 10 s, 6 × 30 s, 5 × 60 s, 5 × 120 s, 4 × 240 s). After a short break of 2-3 minutes a diagnostic CT scan (Visipaque 2 ml/kg) from the superior aspect of the heart to a sub-symphysis level was performed. Static PET imaging (three 5-min bed-positions; cranio-caudal direction) was then performed of the same FOV.

Image analysis

Volumes of interest (VOI) were manually defined (*PMOD software, Zürich, Switzerland*) based on anatomical CT and PET images. VOIs in the prostate were defined on the most tracer-avid hot spot and on reference prostate tissue with low magnitude tracer uptake using a 9-mm brush size in PMOD (**Figure 1B**). VOIs in lymph nodes and bones were placed on lesions with pathologically high tracer uptake.

All VOIs in prostate, lymph nodes, and bones were analysed with respect to their maximum ^{11}C-donepezil standardized uptake values (SUV_{max}), i.e. the measured activity concentration divided by injected radioactivity normalized to body weight. For each patient the lesions with the highest SUV_{max} in prostate, lymph nodes, and bones were selected. Dynamic frames 30-31 representing 24-32 min post-injection were summed before assessment of SUV_{max}, yielding a SUV_{max} estimate at approximately 28 min post-injection. At this time point, the ^{11}C-donepezil time-activity curve in most low-grade PCa has reached a plateau phase.

Kinetic analyses

To obtain further information about tracer behavior in the primary PCa, simplified kinetic modeling of the 36-min dynamic PET was performed. The blood input function was derived from the images using cluster analysis of the pelvic arteries [13]. Time-activity curves of both healthy tissue and tumor tissue were fitted using a reversible 1-tissue (1t2k), an irreversible 2-tissue (2t3k) and a reversible 2-tissue (2t4k) model. No corrections for partial volume effects (PVE) or metabolites were performed. Based on Akaike's information criterion, the reversible 1-tissue model was preferred in 80% of the tumor VOIs and 60% of the healthy tissue. All further analysis was performed using the 1t2k model with K1 describing wash-in and k2 wash-out rates. Using the pelvic image derived input function, the blood signal is expected to be severely underestimated due to partial volume effects leading to systematic error in the derived kinetic parameters. To minimize this error, kinetic parameters are reported as tumor-to-healthy tissue ratios.

Statistical analyses

Statistical analyses were performed using Prism 6 (*Graphpad, La Jolla, California*). SUV_{max} comparisons between group I and II were performed using unpaired t-tests. Correlational analyses between SUV_{max} and Gleason score/PSA were explored with monotonic relationships using Spearman rank correlation coefficient. Comparison of time-activity curves was performed with repeated-measures ANOVA. Results are listed as median (range) or mean ± standard deviation. Statistical significance was defined as $P < 0.05$.

Table 1. Demographic and clinical data

Group	Number of patients	Age (years)	Gleason score (biopsy)	Gleason score (prostatectomy)	PSA (ng/mL)
1	10	64 (52-73)	7 (6-8)	7 (6-9)*	9.0 (5.4-17.2)
2	8	72 (67-80)	8 (7-9)	-	153.0 (56.7-302.7)
3	8	70 (62-81)	-	-	158.6 (0.7-391.0)**

Values are mean (range). *8 of 10 patients in group I had prostatectomy after participating in the study. **One patient in group III had increasing PSA to only 0.7 ng/mL, but se-testosterone, 18F-choline PET and MRI verified castration-resistant PCa. The remaining patients had PSA ranging 32.4-391.0 ng/mL.

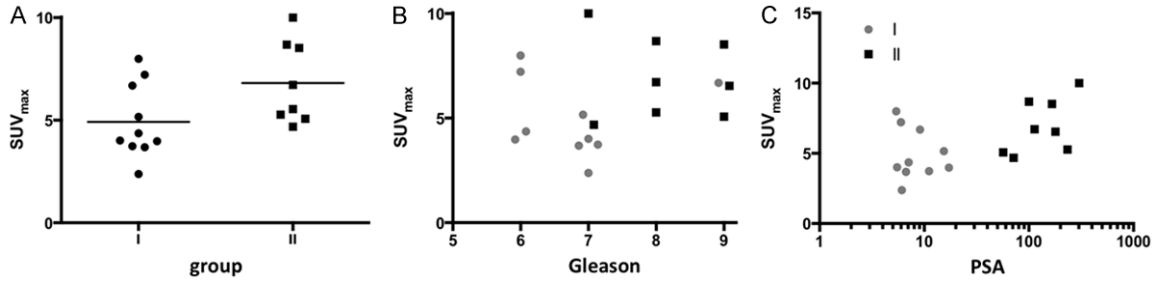

Figure 2. A. SUV_{max} in PCa foci of low-risk (group I) and high-risk patients (group II). B. SUV_{max} in PCa foci in relation to Gleason scores. No correlation was detected. C. A trend-level correlation between SUV_{max} and PSA was seen.

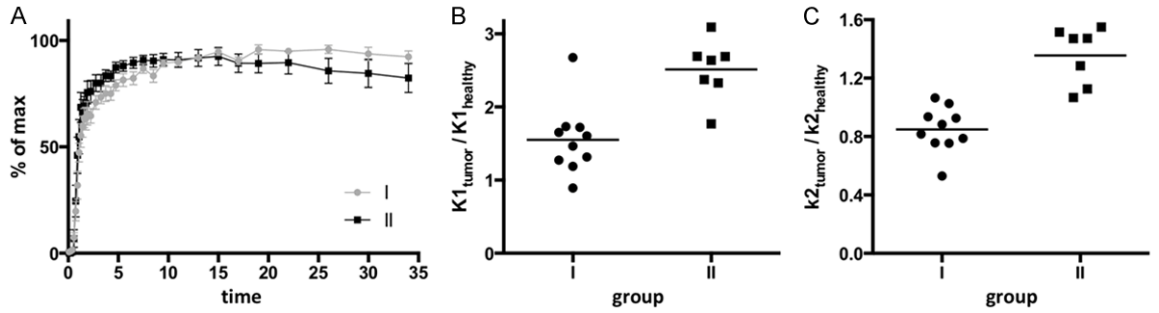

Figure 3. A. Averaged, normalized time-activity curves (mean ± SEM) in low-risk (group I) and high-risk (group II) tumors (P = 0.012, repeated measures ANOVA). B, C. Significant group-differences were seen in K1- and k2-ratios. A healthy tissue VOI could not be defined on one group II PCa, leaving 7 group II cases.

Results

Demographic and clinical data of the patients included are summarized in **Table 1**.

SUV_{max} in groups I and II

The median SUV_{max} in the primary PCa was higher in group II compared to group I, although the difference was only borderline significant (P = 0.052, **Figure 2A**). There was no correlation between Gleason score and SUV_{max} (P = 0.28, **Figure 2B**). A trend-level correlation was seen between PSA and SUV_{max} (P = 0.078, **Figure 2C**). Since group I and II included tumors with partly overlapping Gleason scores (**Figure 2B**), we performed a *post hoc* comparison of SUV_{max} levels in Gleason 6-7 vs. 8-9, which revealed a trend towards higher SUV_{max} levels in the high-grade tumors (P = 0.069; Mann-Whitney).

Kinetic modeling

Slow washout kinetics were generally seen in the primary PCa (**Figure 3A**). A significant difference was seen between the time-activity curves for group I and II with more rapid washout in group II (P = 0.012; repeated measures ANOVA). The 11C-donepezil distribution volume (K1/k2) was significantly higher in group II (grp I: 6.58 ± 2.85, grp II: 10.09 ± 3.86; P = 0.04). Highly significant group differences were seen

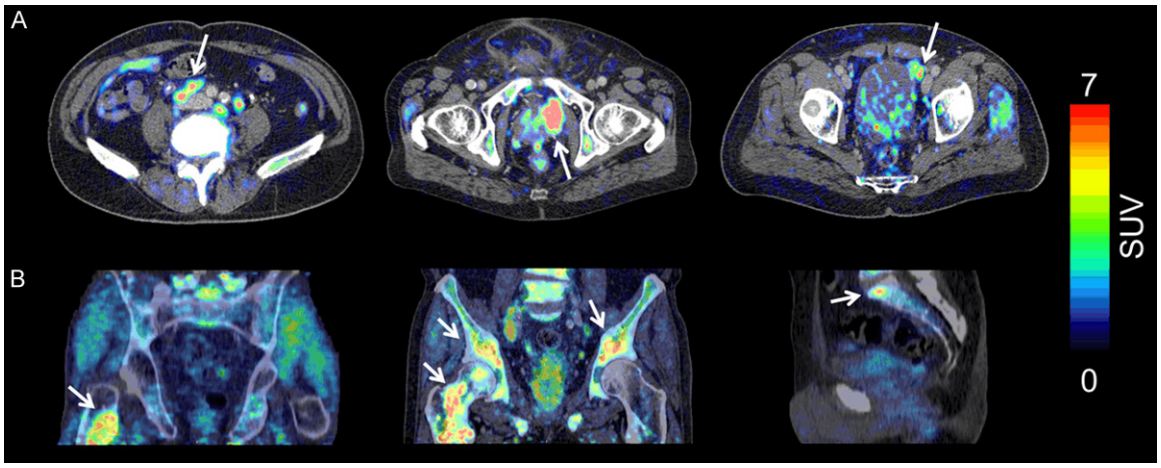

Figure 4. A. Three patients with pathological ^{11}C-donepezil accumulation in lymph nodes. Lymph nodes in the retroperitoneal space (left; SUV_{max} 9.1). Lymph node mass next to the bladder (middle; SUV_{max} 15.8). Single lymph node next to the bladder (middle; SUV_{max} 15.8). B. A representative patient with pathological ^{11}C-donepezil accumulation in suspected, sclerotic bone metastases. Multiple lesions in femoral and pelvic bones (middle; SUV_{max} 11.0 in left acetabulum). [White arrows denote pathological uptake in lymph nodes and bone lesions; yellow arrows denote lymph nodes in A and sclerotic bone lesions in B].

in K1- and k2-ratios between group I and II (P = 0.0006 and P < 0.0001, **Figure 3B**, **3C**).

Metastases

All patients in group III and six patients in group II had lesions characteristic for metastatic disease visualized by ^{11}C-donepezil PET and diagnostic CT. Thus, 14 of 26 patients had pathological lesions outside the prostate. Median SUV_{max} for lesions defined as lymph node metastases was 7.7 (range 4.7-22.5), and for lesions defined as bone metastases the median SUV_{max} was 8.2 (range 5.4-14.8). **Figure 4** shows representative images of ^{11}C-donepezil uptake in lesions suspicious of lymph node and bone metastases.

Discussion

To our knowledge, this is the first *in vivo* PET study to investigate components of cholinergic nerve fibers in PCa tissue. We did not find any significant differences between uptake of ^{11}C-donepezil and tumor aggressiveness, but trends were seen towards higher SUV_{max} in high-risk compared to low-risk patients (P = 0.052), and in Gleason 6-7 vs. 8-9 tumors (P = 0.069). Furthermore, ^{11}C-donepezil showed high uptake in lesions characteristic for metastatic disease.

Several explanations for the observed donepezil uptake are possible. AChE (the target of ^{11}C-donepezil) may be present in higher concentrations in PCa tissue compared to non-PCa tissue, in accordance with a previous report of increased parasympathetic innervation of PCa tissue [9]. It should be emphasized, however, that AChE is not a completely specific marker for cholinergic nerve terminals. It has been demonstrated that immune cells utilize acetylcholine as a non-neuronal signalling molecule, and several immune cells express AChE [14]. Furthermore bacterial abscesses in an infected pig also displayed high peripheral uptake of ^{11}C-donepezil [10]. Thus, the observed increase of ^{11}C-donepezil uptake in PCa could be caused by inflammation or a mixed signal of inflammation and cholinergic innervation. We were aware of this potential bias prior to initiation of the study, and therefore only included patients in whom a minimum of 8 weeks had passed between TRUSb and ^{11}C-donepezil PET, since MRI studies have demonstrated that visible TRUSb-induced inflammation is most often resolved after 8 weeks. A previous autoradiography study showed that ^{11}C-donepezil uptake may also be increased in areas with benign prostate hyperplasia (BPH), but the ^{11}C-donepezil uptake never exceeded that in low-grade cancer foci [12].

Several PET tracers are used in clinical routine for PCa, including ^{18}F-choline, which is superior to the standard oncology tracer ^{18}F-FDG. Nevertheless, the moderate sensitivity and

specificity of choline are not sufficient to accurately stage the primary PCa tumor [15, 16]. More recently, ^{68}Ga-PSMA has been shown to be superior to ^{18}F-choline and other tracers when it comes to primary staging and restaging in biochemical recurrence after radical prostatectomy or salvage therapy [17-22]. ^{68}Ga-PSMA PET can accurately detect lymph node and bone metastases, but the tracer also has limited accuracy to differentiate indolent from aggressive tumors.

In the current study, ^{11}C-donepezil also visualized probable PCa metastases. Although we did not obtain histological verification of these metastases, the anatomical locations of the lesions corresponded to common locations of PCa metastases, including bone metastases in femur, spine and pelvis and lymph node metastases in pelvis and retroperitoneum [23]. In support, a previous study demonstrated that pharmacological blockade of parasympathetic receptors in animal models significantly inhibited metastases formation suggesting a cholinergic component in PCa metastases [9]. Therefore, it is possible that the uptake of ^{11}C-donepezil in lesions suspected for metastases is due to increased cholinergic innervation in the metastases.

All patients in group III were treated with ADT reducing the androgen load on the primary PCa. The effect of ADT on the cholinergic innervation in primary PCa is not known. In general, we observed markedly reduced volume of the prostate glands in group III compared to the two other groups, and very low ^{11}C-donepezil uptake. Therefore, the values of SUV_{max} in the prostate glands in group III are inconclusive.

Our kinetic analyses of the PET data revealed intriguing results. A 1-tissue model was preferred over 2-tissue models in the majority of tumors and healthy tissue. This is contrary to the brain, where previous studies of donepezil kinetics show a clear preference for a 2-tissue model using the same criteria [24]. However, we previously showed that a 1-tissue model had the best performance in most abdominal organs [10]. Of note, the quality of our kinetic analysis may have been impeded by our use of an uncorrected image-derived input function vulnerable to PVE. Nevertheless, the kinetic analysis revealed a number of differences between the groups. The washout parameter k2 was highest in the high-grade tumors. As a result, retention measured using SUV is critically dependent on the time point of the measurement, but the K1 and k2 ratios (**Figure 3B**, **3C**) showed excellent performance in separating group I and II patients. A similar strategy could be feasible using other tracers like ^{68}Ga-PSMA. Of note, the higher K1 and k2 values detected in high-grade tumors are most likely caused in part by the hyperperfusion often present in high-grade prostate cancer. Such hyperperfusion could also contribute to the generally higher SUV_{max} values in high-grade tumors. However, since our published autoradiography data revealed higher ^{11}C-donepezil retention levels in high-grade than low-grade prostate cancers [12], it is also likely that perfusion differences can only partly account for the higher SUV_{max} in high-grade tumors.

Conclusions

^{11}C-donepezil accumulates in primary prostate cancers and most likely also in metastases. The tracer accumulation could be caused by parasympathetic neurogenesis, although sites of inflammation also shows ^{11}C-donepezil uptake. Simple SUV_{max} values of the cancer hot spots were higher in high-risk tumors compared to low-risk tumors, but diagnostic accuracy was insufficient to separate the two groups. In contrast, influx (K1) and efflux (k2) ratios allowed an almost perfect separation between low- and high-risk tumors.

Acknowledgements

Study funded by grants from Danish Cancer Society. The funding body did not play any role in the design of the study and collection, analysis, and interpretation of data or in writing the manuscript.

Disclosure of conflict of interest

None.

Abbreviations

PCa, Prostate carcinoma; PSA, Prostate-specific antigen; TRUSb, Transrectal ultrasound guided needle biopsies; PET, Positron emission tomography; CT, Computerized tomography; AChE, Acetylcholinesterase; ADT, Androgen deprivation therapy; i.v., Intra-venous; VOI,

Volumes of interest; SUV_{max}, Maximum standardized uptake value; FOV, Field-of-view; PVE, Partial volume effects; BPH, Benign prostate hyperplasia.

Address correspondence to: Dr. Per Borghammer, Department of Nuclear Medicine and PET, Aarhus University Hospital, Palle Juul-Jensens Boulevard 165, J220, Aarhus N 8200, Denmark. E-mail: perborgh@rm.dk

References

[1] Siegel RL, Miller KD, Jemal A. Cancer statistics, 2015. CA Cancer J Clin 2015; 65: 5-29.

[2] Sakr WA, Grignon DJ, Crissman JD, Heilbrun LK, Cassin BJ, Pontes JJ, Haas GP. High grade prostatic intraepithelial neoplasia (HGPIN) and prostatic adenocarcinoma between the ages of 20-69: an autopsy study of 249 cases. In Vivo 1994; 8: 439-43.

[3] Wilt TJ, Brawer MK, Jones KM, Barry MJ, Aronson WJ, Fox S, Gingrich JR, Wei JT, Gilhooly P, Grob BM, Nsouli I, Iyer P, Cartagena R, Snider G, Roehrborn C, Sharifi R, Blank W, Pandya P, Andriole GL, Culkin D, Wheeler T; Prostate Cancer Intervention versus Observation Trial (PIVOT) Study Group. Radical prostatectomy versus observation for localized prostate cancer. N Engl J Med 2012; 367: 203-13.

[4] Aus G, Abbou CC, Bolla M, Heidenreich A, Schmid HP, van Poppel H, Wolff J, Zattoni F. EAU guidelines on prostate cancer. Eur Urol 2005; 48: 546-51.

[5] Isariyawongse BK, Sun L, Banez LL, Robertson C, Polascik TJ, Maloney K, Donatucci C, Albala D, Mouraviev, Madden JF, Moul JW. Significant discrepancies between diagnostic and pathologic gleason sums in prostate cancer: the predictive role of age and prostate-specific antigen. Urology 2008; 72: 882-6.

[6] Norberg M, Egevad L, Holmberg L, Sparen P, Norlen BJ, Busch C. The sextant protocol for ultrasound-guided core biopsies of the prostate underestimates the presence of cancer. Urology 1997; 50: 562-6.

[7] Ganzer R, Stolzenburg JU, Wieland WF, Brundl J. Anatomic study of periprostatic nerve distribution: immunohistochemical differentiation of parasympathetic and sympathetic nerve fibres. Eur Urol 2012; 62: 1150-6.

[8] Witte LP, Chapple CR, de la Rosette JJ, Michel MC. Cholinergic innervation and muscarinic receptors in the human prostate. Eur Urol 2008; 54: 326-34.

[9] Magnon C, Hall SJ, Lin J, Xue X, Gerber L, Freedland SJ, Frenette PS. Autonomic nerve development contributes to prostate cancer progression. Science 2013; 341: 1236361.

[10] Gjerloff T, Jakobsen S, Nahimi A, Munk OL, Bender D, Alstrup AK, Vase KH, Hansen SB, Brooks DJ, Borghammer P. In vivo imaging of human acetylcholinesterase density in peripheral organs using 11C-donepezil: dosimetry, biodistribution, kinetic analyses. J Nucl Med 2014; 55: 1818-24.

[11] Gjerloff T, Fedorova T, Knudsen K, Munk OL, Nahimi A, Jacobsen S, Danielsen EH, Terkelsen AJ, Hansen J, Pavese N, Brooks DJ, Borghammer P. Imaging acetylcholinesterase density in peripheral organs in parkinson's disease with 11C-donepezil PET. Brain 2015; 138: 653-63.

[12] Stokholm MG, Hoyer S, Borre M, Bender D, Jakobsen S, Frokiaer J, Borghammer P. Molecular imaging of cholinergic processes in prostate cancer using 11C-donepezil and 18F-FEOBV. Eur J Nucl Med Mol Imaging 2016; 43: 906-10.

[13] Harms HJ, Knaapen P, de Haan S, Halbmeijer R, Lammertsma AA, Lubberink M. Automatic generation of absolute myocardial blood flow images using [15O]H2O and a clinical PET/CT scanner. Eur J Nucl Med Mol Imaging 2011; 38: 930-9.

[14] Kawashima K, Fujii T, Moriwaki Y, Misawa H. Critical roles of acetylcholine and the muscarinic and nicotinic acetylcholine receptors in the regulation of immune function. Life Sci 2012; 91: 1027-32.

[15] Picchio M, Mapelli P, Panebianco V, Castellucci P, Incerti E, Briganti A, Gandaglia G, Kirienko M, Barchetti F, Nanni C, Montorsi F, Gianolli L, Fanti S. Imaging biomarkers in prostate cancer: role of PET/CT and MRI. Eur J Nucl Med Mol Imaging 2015; 42: 644-55.

[16] Kitajima K, Murphy RC, Nathan MA. Choline PET/CT for imaging prostate cancer: an update. Ann Nucl Med 2013; 27: 581-91.

[17] Eiber M, Maurer T, Souvatzoglou M, Beer AJ, Ruffani A, Haller B, Graner FP, Kübler H, Haberkorn U, Eisenhut M, Wester HJ, Gschwend JE, Schwaiger M. Evaluation of hybrid (6)(8)Ga-PSMA ligand PET/CT in 248 patients with biochemical recurrence after radical prostatectomy. J Nucl Med 2015; 56: 668-74.

[18] Hijazi S, Meller B, Leitsmann C, Strauss A, Meller J, Ritter CO, Lotz J, Schildhaus HU, Trojan L, Sahlmann CO. Pelvic lymph node dissection for nodal oligometastatic prostate cancer detected by 68Ga-PSMA-positron emission tomography/computerized tomography. Prostate 2015; 75: 1934-40.

[19] Afshar-Oromieh A, Haberkorn U, Schlemmer HP, Fenchel M, Eder M, Eisenhut M, Hadaschik BA, Kopp-Schneider A, Röthke M. Comparison of PET/CT and PET/MRI hybrid systems using a 68Ga-labelled PSMA ligand for the diagnosis of recurrent prostate cancer: initial experience. Eur J Nucl Med Mol Imaging 2014; 41: 887-97.

[20] Mease RC, Foss CA, Pomper MG. PET imaging in prostate cancer: focus on prostate-specific membrane antigen. Curr Top Med Chem 2013; 13: 951-62.
[21] Bouchelouche K and Choyke PL. Prostate-specific membrane antigen positron emission tomography in prostate cancer: a step toward personalized medicine. Curr Opin Oncol 2016; 28: 216-21.
[22] Afshar-Oromieh A, Holland-Letz T, Giesel FL, Kratochwil C, Mier W, Haufe S, Debus N, Eder M, Eisenhut M, Schäfer M, Neels O, Hohenfellner M, Kopka K, Kauczor HU, Debus J, Haberkorn U. Diagnostic performance of (68)Ga-PSMA-11 (HBED-CC) PET/CT in patients with recurrent prostate cancer: evaluation in 1007 patients. Eur J Nucl Med Mol Imaging 2017; 44: 1258-68.
[23] Bubendorf L, Schopfer A, Wagner U, Sauter G, Moch H, Willi N, Gasser TC, Mihatsch MJ. Metastatic patterns of prostate cancer: an autopsy study of 1,589 patients. Hum Pathol 2000; 31: 578-83.
[24] Hiraoka K, Okamura N, Funaki Y, Watanuki S, Tashiro M, Kato M, Hayashi A, Hosokai Y, Yamasaki H, Fujii T, Mori E, Yanai K, Watabe H. Quantitative analysis of donepezil binding to acetylcholinesterase using positron emission tomography and [5-(11)C-methoxy]donepezil. Neuroimage 2009; 46: 616-23.